Desalination and Water Treatment
www.deswater.com

doi: 10.5004/dwt.2022.29112

280 (2022) 32–43
December

Improved production from an air gap membrane distillation desalination system by varying the feed entry angle and coolant plate geometry

Mohammad Jabed Perves Bappy[a], Rubina Bahar[b,*]

[a]*Micro and Nanoscale Systems Engineering, Louisiana Tech University, 201 Mayfield Ave, Ruston, LA 71272, Louisiana, USA, Tel.: +1 (318) 278 5729; email: mjb071@latech.edu*
[b]*Department of Mechanical and Materials Engineering, Universiti Tunku Abdul Rahman, Sungai Long, Cheras, Kajang 43000, Malaysia, email: rubina@utar.edu.my*

Received 14 December 2021; Accepted 4 November 2022

ABSTRACT

Air gap membrane distillation (AGMD) is an emerging technique to produce freshwater using low-grade heat as the process is driven by the partial pressure difference between two dissimilar temperature liquids. This study tested an innovative technique to minimize polarization and increase production from an AGMD lab-scale unit. The effect of the feed flow entry angle has been investigated. A specially designed coolant plate with 60 fins has been fabricated, and detailed theoretical and simulation studies of condensation over the special geometry coolant plate have been conducted. Also, the combined effect of inclined flow entry and a finned coolant surface has been studied experimentally. The experiments show that with a feed flow entry angle of 60°, the system achieves an average of 10% to 14% boost in performance. When the 60° inlet flow angle and finned coolant plate work in combination, an average of 69% to 78% increase in distillate flux was observed with the same energy input.

Keywords: Membrane distillation (MD) desalination; Air gap membrane distillation (AGMD); Feed entry angle; Polarization; Finned coolant plate

1. Introduction

Freshwater demand is increasing each year with population growth. Six Gulf Co-operation Council (GCC) countries have already gone down to the freshwater scarcity line for having renewable water resources <1,000 m^3/y·cap, as stated by World Health Organization (WHO). Many Asian counties are at risk. Almost all Middle Eastern countries are starting to depend on desalination techniques to augment their freshwater supply [1]. There are nearly 16,000 desalination plants worldwide with a desalination capacity of 95 million m^3/d [2]. Current water production methods like reverse osmosis or multi-effect distillation are energy and land-intensive processes. So, membrane distillation (MD) has been gaining popularity over the last few decades as an energy-efficient and cost-effective process to purify water from saline water. Membrane distillation-based water treatment started to surface in the early '80s as a viable solution for drinking water scarcity. Membrane distillation (MD) is an evaporation process between a hot liquid and a cold condensation medium that is driven by partial pressure difference. It does not involve boiling, and a hydrophobic membrane is placed on the evaporating surface through which only vapour can travel from the hot feed solution toward the condensation medium. The process provides the freedom of less sensitivity to feedwater concentration. At the same time, low operating temperature and pressure make it suitable to utilize industrial waste heat and solar energy as heat sources [3–6].

* Corresponding author.

Various categories of MD processes have been developed since the innovation of the basic technique in the 1960s. Direct contact membrane distillation (DCMD), sweeping gas membrane distillation (SGMD), and vacuum membrane distillation (VMD) are some usual techniques in use for decades. In DCMD, there is no air gap. The vapour is condensed directly in a cold distilled water stream which flows by touching the surface of the membrane [7]. An inert gas is flowed to collect the vapour in the SGMD process. In contrast, the vapour is collected by creating a vacuum in the permeate side of the membrane in the VMD process [8]. Among these categories, air gap membrane distillation (AGMD) maintains a narrow air gap between the hot liquid and the condensation surface. It preserves the thermal energy for the process to continue further. AGMD system offers better insulation between the evaporating and condensing surface. The thermal efficiency of AGMD can reach up to 90% [9], and the process also provides a barrier between the permeate and the coolant fluid through a solid coolant plate. Thus, the coolant fluid can be any liquid at a lower temperature than the feed solution, with a lower chance of permeate contamination. Unlike DCMD, AGMD is free of pollution by leakage problems. Also, AGMD offers the benefit of maximum internal heat recovery and reduces heat loss by conduction compared to all these membrane distillation (MD) techniques [6]. Because of these lucrative benefits over other MD techniques, the AGMD system covers a vast range of applications such as water purification, ion separation, and desalination [10].

Although the AGMD process seems attractive as a convenient water treatment method, the system still has significant room for improvement in production, reduced temperature and concentration polarization, and membrane cost and durability. After the apparent resistance by the membrane itself, temperature and concentration polarization remain the main factors that reduce the mass flux in the AGMD process. Temperature polarization occurs due to the reduction of temperature near the evaporation or condensation surface of the AGMD process as a large amount of heat is consumed and resealed at the time of phase transition. So, it causes the membrane surface temperature to differ from the measured balk temperature of the two sides of the membrane [11]. Moreover, when the concentration of the feed solution rises, especially in the case of seawater, we need to consider the concentration polarization as a primary source of the reduction of the driving force [12]. The production rate of the process can be increased significantly by reducing the effect of polarization [13].

AGMD process has drawn the attention of researchers, and different enhancement techniques are associated with the process in contemporary water research. Studies on the effects of feed and coolant temperature, feed concentration, air gap width, and flow orientation on productivity and energy consumption have already been covered through numerous research works in the previous two decades. In recent years, more focused research has been carried out to improve the AGMD system by minimizing the polarization [14], energy utilization through multi-staging [15–17]; improving the condensation process [18–20] and other techniques [21–23]. It has been found from a thorough literature search that very few works are reported on the condensation plate's structure, and no work has been reported about the feed's entry angle into the feed chamber other than our previous work [24]. Literature showed that some researchers tried to tilt the whole module vertically at a slight angle, but nobody had previously attempted to modify the inlet angle [25]. Therefore, there is enough scope for investigating the effect separately and in combination to find the improvement that can bring to production.

This work presents the effect of an inclined entry to the feed chamber to minimize polarization. A finned coolant plate has also been used to increase the condensation rate keeping the energy input the same. A lab-scale AGMD unit has been fabricated, and experiments have been conducted with variable feed and coolant temperatures. Simulation studies have been conducted to understand condensation over a finned coolant plate better.

2. Theory

Heat and mass transfer co-occur by conduction and convection in the AGMD process. The vapour transmission through the air gap can be considered pure diffusion and conduction, whereas convection can be ignored for a very high Rayleigh number. The condensation on the coolant plate depends vastly upon the efficiency and effectiveness of the fins. In this study, a brief theoretical framework has been developed to understand the condensation process on the finned coolant plate, while the effect of entry angle has been studied mostly by experiments. The basic model of an AGMD system is shown in Fig. 1. The modeling of the system needed to be concentrated on the fin effects and fin geometry to modify the AGMD system for better performance. Condensation over a vertical plate was also studied to set the temperature parameters.

2.1. 2-D vapour transportation in AGMD

The 2-D vapour transportation of the AGMD process can be expressed as the terms of temperature by using Antoine's correlation for pure water where:

$$\log P_W = A - \frac{B}{C + T_W} \tag{1}$$

where P_w and T_w is the vapour pressure and temperature of pure water, respectively, where the driving potential:

$$\Delta P = P_{W1} \sim P_{W2} \tag{2}$$

where A, B and C component specific constant for pure water. For saline water, the value of P_w is corrected using Raoult's law as:

$$P_W = \left(1 - \mathrm{CM}_{\mathrm{NaCl}}\right) P_{\text{pure water}} \tag{3}$$

where $\mathrm{CM}_{\mathrm{NaCl}}$ = mole solute concentration.

Now, the diffusion rate throughout the membrane depends upon the concentration of the component. According to Fick's Law, the mass flux of a constituent per unit area is proportional to the concentration gradient.

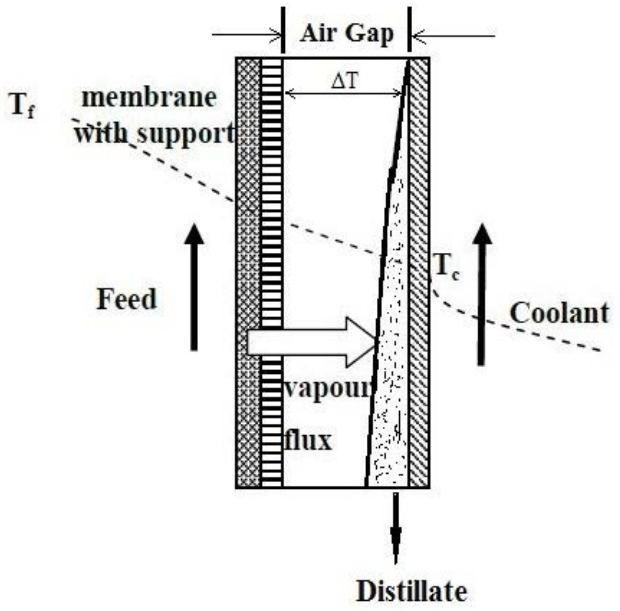

Fig. 1. Basic model of AGMD system.

$$\frac{\dot{m}_A}{A} = -D\frac{\partial C_A}{\partial x} \tag{4}$$

where D is the diffusion coefficient, $\dot{m}_A$ is mass flux per unit time, and C_A is the mass concentration of component A per unit volume.

Again, according to Stefan's law of diffusion, the total mass flow of water vapour:

$$\hat{m}_{W,\text{total}} = \frac{D_p M_w A}{R_o T\left(X_2 - X_1\right)} \tag{5}$$

where $X_2 - X_1$ = thickness of air (distance to travel), A = total surface area, D = diffusion coefficient, M_w = molecular weight of water, R_o = universal gas constant, and T = temperature.

2.2. Heat and mass transfer through air gap

The transport of vapour through the air gap and membrane pores can be described by molecular diffusion theory. A stagnant air film zone is assumed inside the air gap of the AGMD system. The transport of vapour molecules through this stagnant air zone is a laminar flow that occurs for molecular diffusion. The Fick's law of diffusion can determine the rate of diffusion:

$$N_v = -D\frac{dC_v}{d_x} \tag{6}$$

where N_v is the rate of diffusion of vapour molecule through the air gap, D is diffusivity, C_v is the concentration of vapour, and x is the air gap distance. The negative sign arises as the concentration of vapour decreases as the air gap increases.

If the air gap is below 5 mm, then the flux through the membrane and through the air gap calculated for one-directional flow can be expressed by the Eq. (7) [26]:

$$J = \frac{\text{PM}}{\text{RTP}_w}\left(\frac{D}{\frac{\delta}{\varepsilon^{3.6}} + 1}\right)\Delta p \tag{7}$$

where Δp is the vapour pressure difference between the membrane feed and the condensation surface. P_w is the partial pressure of water.

The total mass flow of water vapour through air gap can be calculated by Stefan's law of molecular diffusion [27]:

$$\dot{M}_{w,\text{total}} = \frac{\text{DPM}_w A}{\text{RTX}}\frac{dP_w}{dy} \tag{8}$$

where A is the area, x is the air gap, and D is the diffusion coefficient.

The vapour flow through the air gap is also slightly affected by the natural convection in the air gap. Natural convection happens for the temperature difference on the two sides of the gap. The importance of the natural convection depends upon the Rayleigh number [28]:

$$R_a = \frac{g\beta\Delta T_x \delta_x^3}{v_a \alpha_a} \tag{9}$$

where ΔT_x is the temperature difference in the two sides of the air gap, δ_x is the air gap, β is the thermal expansion coefficient, g is the gravitational acceleration, and V_a and α_a are the kinematic viscosity and thermal diffusivity of air, respectively. From the calculation, if R_a is less than 1,000, then the natural convection can be neglected compared to conductive heat transfer through the air gap [29]:

The conductive heat transfer inside the gap can be expressed as:

$$Q = \left(\frac{K_a A}{t} + \dot{m}c\right)\Delta T \tag{10}$$

where K_a is the thermal conductivity of air, A is the effective heat transfer area, $\dot{m}$ is the mass flux, and ΔT is the temperature difference between the two sides of the air gap.

2.3. Fin efficiency

Fin efficiency can be determined by the Eq. (11):

$$\eta_{\text{fin}} = \frac{Q_{\text{fin}}}{Q_{\text{fin max}}} = \frac{\text{Rate of actual heat transfer of the fin}}{\text{Rate of ideal heat transfer from the fin}} \tag{11}$$

where η_{fin} = efficiency of the fin and Q_{fin} = actual heat transfer rate of the fin.

The equation considered that the entire fin is on its base temperature. That means, in the case of very low thermal resistance and very high thermal conductivity, the temperature of the fin is assumed to be uniform all over its body same as its base value [30]:

$$Q_{\text{fin}} = \eta_{\text{fin}} \times Q_{\text{fin max}} = \eta_{\text{fin}} h A_{\text{fin}}\left(T_b - T_\infty\right) \tag{12}$$

In the case of determining the efficiency of the coolant plate used in this experiment, the finned area and the un-finned area both needed to be considered in the calculation. So the surface of the coolant plate having n number of fins can be generally expressed as seen in Fig. 2.

$$Q_{\text{total, fin}} = Q_{\text{unfin}} + Q_{\text{fin}} = h\left(A_{\text{unfin}} + \eta_{\text{fin Afin}}\right)\left(T_b - T_\infty\right) \tag{13}$$

where A_{fin} is the area of the finned portion of the surface and A_{unfin} expresses the un-finned portion of the area of the coolant plate surface. $Q_{\text{total,fin}}$ is expressing the total heat transfer from the coolant plate [30].

2.4. Fin effectiveness

The fin effectiveness determines the extra facility achieved from the fin than the un-finned surface in terms of heat transfer. So the fin effectiveness can be expressed as:

$$\varepsilon_{\text{fin}} = \frac{Q_{\text{fin}}}{Q_{\text{unfin}}} = \frac{Q_{\text{fin}}}{hA_{\text{fin}}\left(T_b - T_\infty\right)} = \frac{\text{rate of heat transfer of the fin from the base area } A_b}{\text{rate of heat transfer from the surface of the fin are } A_b} \tag{14}$$

The significance of ε_{fin} will suggest the necessity of using fin in this experiment.

If $\varepsilon_{\text{fin}} = 1$, then the use of finned surface does not affect the performance of the coolant plate at all. $\varepsilon_{\text{fin}} < 1$ means that the finned surface of the coolant plate is acting as an insulator and will not increase the performance of the plate. It can happen if low k material has been used as fin material. And if $\varepsilon_{\text{fin}} > 1$, then the fin is giving better effectiveness in terms of heat transfer for the coolant plate, and the use of fins will enhance the performance of the coolant plate rather than using a simple flat plate [27].

So, it can be deduced that the overall effectiveness of a finned surface can be measured by the ratio of the total heat transfer from the finned surface to the ratio of heat transfer of the same surface if that was flat with no fins.

$$\varepsilon_{\text{fin,overall}} = \frac{Q_{\text{total fin}}}{Q_{\text{total unfin}}} = \frac{h\left(A_{\text{unfin}}\eta_{\text{fin}}A_{\text{fin}}\right)\left(T_b - T_\infty\right)}{hA_{\text{unfin}}\left(T_b - T_\infty\right)} \tag{15}$$

The effectiveness of fins is high, where h is relatively low. Copper, aluminum, and iron have relatively high effectiveness, whereas aluminum is preferred for this study, considering its easy machinability, high resistance to corrosion, and low weight and cost.

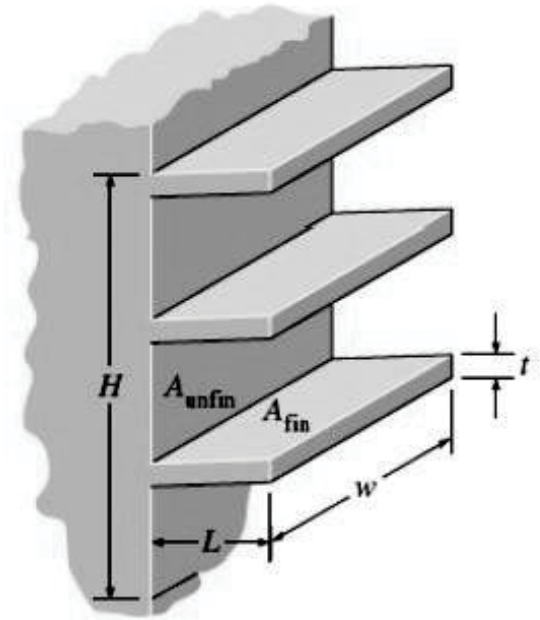

Fig. 2. Calculation of fin efficiency.

3. Materials and methods

3.1. Simulation study of the finned condensation plate

In multiphase flow, the Eulerian wall film model is a popular one to understand the behavior in such conditions of the study. ANSYS Fluent software package was used to study the simulation process. The main governing equations for the simulation process used are given below.

3.1.1. Momentum equation

The primary momentum equation follows in the wall film phase change model is:

$$\rho h\overline{\frac{du_p}{dt}} + h_f\left(\Delta\text{spf}\right)\alpha = \tau_g\overline{t_g} + \tau_w\overline{t_w} + \overline{\dot{P}_{\text{imp},\alpha}} - \dot{M}_{\text{imp},\alpha}\overline{U_p} + \overline{\dot{F}_{n,a}} + \rho h\left(\overline{g} - a_w\right) \tag{16}$$

where α denotes the current face on which the particle resides, h_f denotes the current film height at the particle location, Δ_s is the gradient operator restricted to the surface, and p_f is the pressure on the surface of the film [31].

3.1.2. Passive scalar equation

Transport equation for a passive scalar in wall film is given by:

$$\frac{\partial\rho hY}{\partial t} + \Delta_s\left(\rho_1 h_f\overline{V_1}Y\right) = \Delta_s\left[\Gamma\Delta_S\left(h_f Y\right)\right] + \dot{m}_s \tag{17}$$

where Y = arbitrary passive scalar, h_f = film height, $\overline{V_1}$ = mean film velocity, ρ_1 = liquid density, $\dot{m}_s$ = scalar related mass source term per unit area, Γ = diffusivity for the scalar.

3.1.3. Mass conversion equation

Conservation of mass for a two-dimensional film in a three-dimensional domain is:

$$\frac{\partial\rho_1 h}{\partial t} + \Delta_s\left(\rho_1 h_f\overline{V_1}\right) = \dot{m}_s \tag{18}$$

where ρ_1 is the liquid density, h_f the film height, Δ_s the surface gradient operator, $\overline{V_1}$ the mean film velocity, and $\dot{m}_s$ the mass source per unit wall area due to droplet collection, film separation, film stripping, and phase change [31].

3.1.4. Conversion of momentum

Conservation of film momentum is given:

$$\frac{\partial \rho h \overline{V_1}}{\partial t} + \Delta_s\left(\rho_1 h_f \overline{V_1}\,\overline{V_1} + \overline{D_V}\right) = -h_f \Delta_s P_L + \rho h \overline{g_\tau} + \frac{3}{2}\tau\overline{fs} - \frac{3u_1}{h_f}\overline{V_1} + \dot{q} \tag{19}$$

The terms on the left-hand side of Eq. (19) represent transient and convection effects, respectively, with tensor $\overline{D_V}$ denoting the differential advection term computed based on the quadratic film velocity profile representation. On the right-hand side, the first term includes the effects of gas-flow pressure, the gravity component normal to the wall surface (known as spreading), and surface tension. The second-term represents the effect of gravity in the direction parallel to the film; the third and fourth terms represent the net viscous shear force on the gas-film and film-wall interfaces, based on the quadratic film velocity profile representation. And the last term is associated with droplet collection or separation. A parabolic film velocity profile has been assumed in arriving at the shear and viscous terms on the RHS [32]. A three-dimensional Eulerian wall film multiphase model was chosen to simulate the process with phase accretion, enabling phase change. The Eulerian multiphase model is the best choice for condensation modeling on flat plates when phase change happens. The 3D computational domain was used by activating double precision to investigate the plate's volume fraction of condensate mass. The set-ups and boundary conditions of the simulation are shown in Table 1.

Pressure based solver was used on a transient condition where a viscous model has been considered as laminar flow. The phase change from liquid water to vapour has been defined where liquid water was selected as the primary phase, and vapour was defined as the secondary phase material. The nodal solution of the simulation process is shown in Fig. 3 with the grid dimension of the plate.

The process was run for coolant temperatures 10°C, 15°C, 20°C, 25°C, and 30°C where the feed temperature varies at 40°C, 45°C, 50°C, 55°C, 60°C, 65°C, and 70°C for each run. One thousand iterations run for each solution domain. The contour plot vapour fraction of the channeled coolant plate is shown in Fig. 4 after 1 min for transient flow at 10°C coolant temperature and 70°C feed temperature.

The result section of the fluent solver gives additional results of the simulations like mass and weight of vapour particles, heat transfer rate, flux, etc., which have been imported in a text file to compare with experimental results.

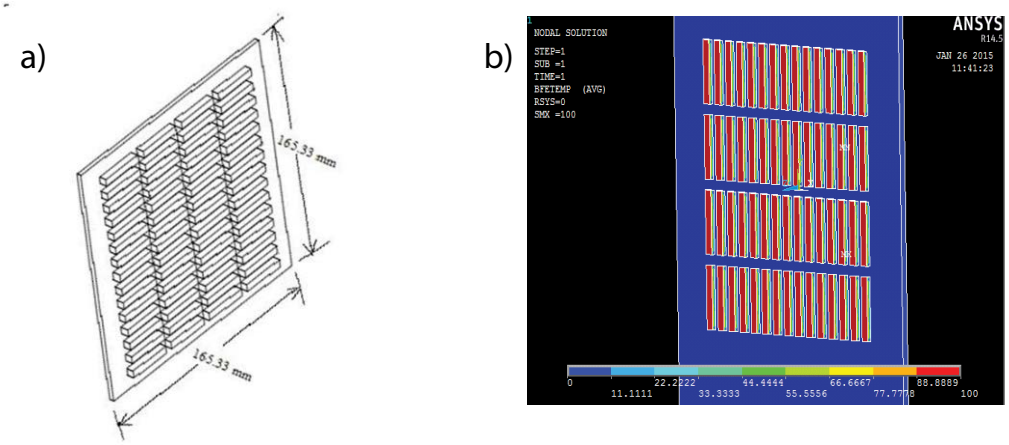

Fig. 3. (a) Dimension of the design grid and (b) nodal solution of the design grid.

Table 1
Simulation set-ups and boundary conditions

Simulation set-ups		Boundary conditions	
Model	Multiphase Eulerian wall film	Hot feed temperatures (inlet) (°C)	40~70@5°C
Solver type	Pressure-based	Cold feed temperature (outlet) (°C)	10~30@5°C
Time study	Transient	Wall temperature (°C)	25
Viscous model	Laminar	Membrane effective area (cm^2)	88.2
Primary phase	Vapour	Vapour volume flow rate (mL/min·cm^2)	35
Secondary phase	Water	Number of iterations	1,000

3.2. Experimental set-up

The membrane module contained two chambers, one containing the hot feed and the other with the coolant. The module casing was made from 5 mm thick polycarbonate sheets, and the dimensions of the hot and cold chamber were approximately 162 mm × 162 mm × 106 mm. It included six parts: as seen in Fig. 5a.

The experimental set-up is shown in Fig. 5b, indicating the significant parts. The recirculation heater heated the salt water for the hot side and sent it to the feed side with the increased temperature. On the other side, a recirculation cooling bath was supplying cold tap water as the coolant. A polytetrafluoroethylene (PTFE) hydrophobic membrane was used as the barrier between the hot feed and the coolant. The condensate plate was made of aluminum for easy fabrication of fins. A finned coolant plates were used as it has been proven to produce higher distillate compared to a plain coolant plate in recent studies [33,34]. Fig. 5c shows the finned coolant plates. The staggered fins included 60 numbers of shorter 30 mm rectangular fins, respectively. Fig. 5d shows the PTFE membrane with built-in support to prevent the membrane from bulging during the feed flow over it. The food-grade colour was mixed with the feed to detect any leakage by checking the colour tint of the distillate. Sixteen thermocouples were used to measure the temperatures, and the data were recorded using a data logger.

The membrane was attached to the chambers through a membrane holder ramp, and it has a slight annular depression machined to accommodate the membrane. A notch was machined at the bottom of the membrane holder, so a hollow cavity will be formed to let the condensate come out when attached to the hot and cold side. The condensate was collected in a graduated beaker to record the water production rate.

3.3. Experimental variables

After initial testing and ensuring no leakage, the experiments were conducted with variable feed and coolant temperatures. Table 2 shows the apparatus used and Table 3 shows the operating variable ranges.

Before running the experiments, a simulation study was required to decide on the optimum entry angle, as multiple drillings at the entrance for different angles would not be possible. Therefore, a flow simulation inside the hot solution chamber was conducted to find the best impact angle of the inlet pipe so that maximum flow circulation occurs around the membrane area. If the hot water is poorly circulated on the membrane surface, then stagnation may happen, and the membrane would lose its productivity caused by temperature and concentration polarization. The membrane was placed precisely in the middle of the wall, so it was necessary to find an angle for the inlet pipe to make sure the flow could strike mildly toward the membrane side area of the wall. Also, it was kept in mind that the water flow should not hit the membrane, or it may rupture. Therefore, the perfect angle needed to be determined for the final experiments through an ANSYS fluent simulation. Fig. 6 shows the entry angle arrangement.

3.4. Experimental uncertainty analysis

As per the theory discussed in section 2, the overall production is dominated by the partial pressure difference, which is directly related to the temperature of the hot and cold sides. The pressure was not measured as the system worked under environmental pressure, and there was no chance of pressure variation across the set-up. Therefore, only temperature sensing devices can be linked to the existing uncertainty in the production. K-type thermocouples were used to measure the temperature with +0.1°C accuracy. Therefore, the only instrument error $dT_1 = \pm 0.1$°C is the uncertainty associated with the thermocouples, the random error δT_2 can be expressed as, $\sum_1^n \frac{T-\bar{T}}{n-1}$, here, n = number of data taken to determine T, $\bar{T}$ is the mean value. The total error associated with temperature can be summarized as $(\delta T_1^2 + \delta T_2^2)^{0.5}$.

4. Results and discussion

4.1. Effect of different types of coolant plates

The experiment progressed with variations in the geometry of the coolant plate. Fig. 7a shows the distillate

Table 3
Operating variables

Operating variables	Values (range)
Feed temperature, °C	40~70@5°C interval
Coolant temperature, °C	10~30@5°C interval
Coolant plate design	Plain and staggered finned
Air gap, mm	2 mm
Flow rate, L/min	2

Table 2
Apparatus/materials

Apparatus/materials	Specification/range	Brand
PTFE membrane	142 mm diameter and 0.45 μm pore-size maximum temperature~80°C	MF Millipore
Recirculation baths for flow system	5 L capacity, maximum pump flow 15 L/min, temperature range –25°C~100°C	LAUDA Alpha RA 8
Temperature sensors	K-type with temperature range: 0°C~480°C	HEATWATT with 32 channels
Coolant plate	Aluminum coolant plate with fins	–
Hot feed solution	Salt (NaCl) water solution with a salinity of 44 g/L	–

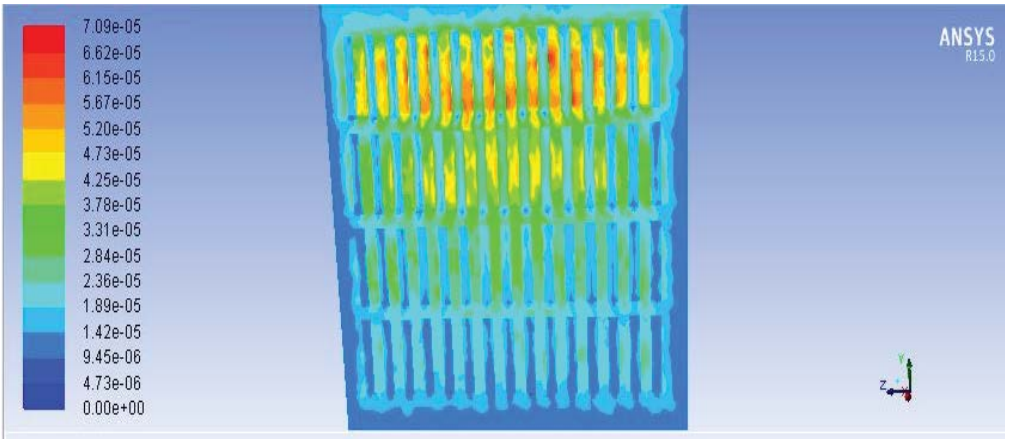

Fig. 4. Vapour fraction contour plot of the channeled coolant plate at 1 min transient time.

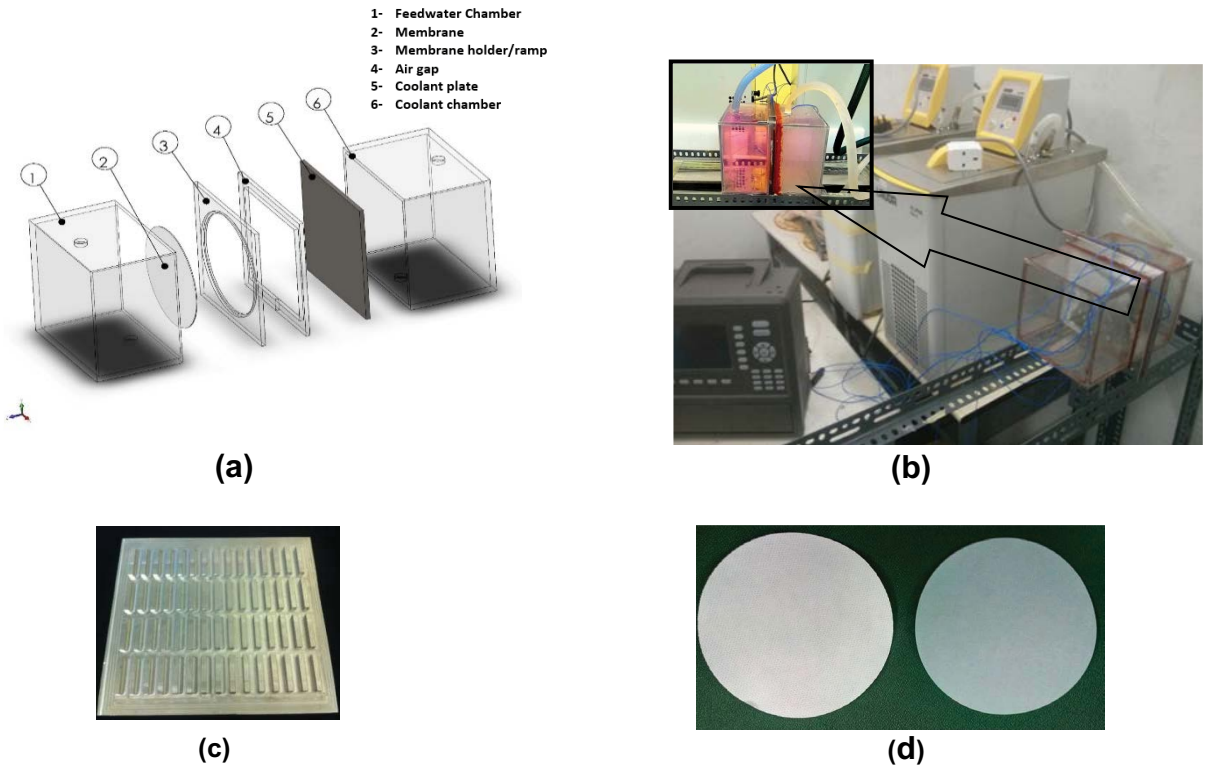

Fig. 5. (a) Schematic of the module with different parts, (b) overall experimental set-up, (c) finned condensation plates and (d) PTFE membrane with built-in support.

production with varying feed temperature and coolant temperature for a flat coolant plate, while Fig. 7b shows the production using the finned coolant plate. It can be observed from the figures that almost 7.4 kg/m^2·h distillate flux was obtained in the same condition for the finned plate, where the flat one gives a maximum of 5.1 kg/m^2·h at 70°C feed side temperature and 10°C coolant side temperature. On average, around 40%–45% increase in distillate flux has been achieved after using fins on the coolant plate surface. The reason may be attributed to the fact that although the MD process is dominated by temperature difference hence the partial pressure difference across the membrane; in this case, the surface area of condensation has been increased, and therefore, more vapour was able to condense, making room for more vapour to come in and condense on the finned coolant plate. Moreover, the extended cross-sectional area of the fins increased the overall thermal effect of the system. In both cases, a straight feed entry angle was used.

4.2. Determination of the optimum entry angle

A flow simulation was conducted using ANSYS Fluent software, and it was found that the 60° angle was good enough as the inlet pipe angle that covers the most suitable

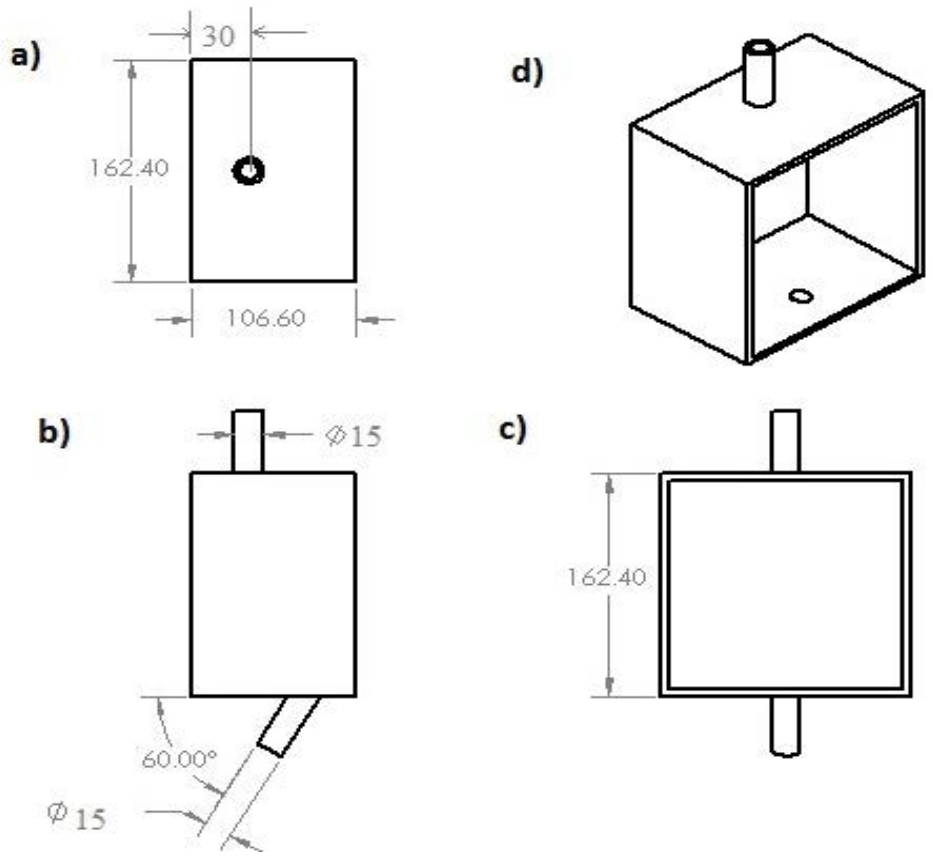

Fig. 6. Feedwater chamber (a) from the bottom, (b) from the front, (c) from the side and (d) isometric.

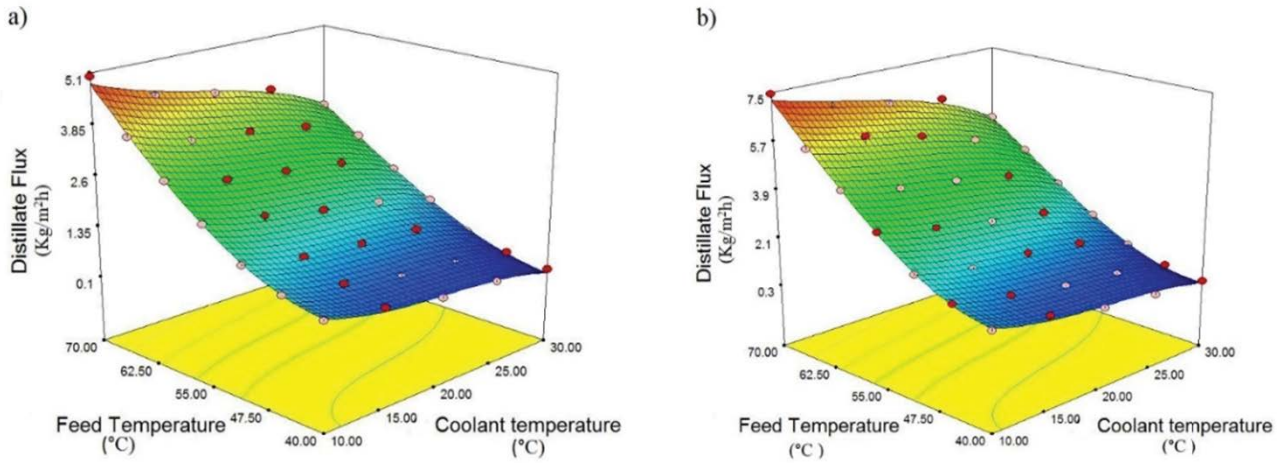

Fig. 7. Surface plot of distillate output with straight inlet flow (a) plain coolant plate and (b) finned coolant plate.

'washing effect' on the membrane. Considering the risk factor of the membrane rupture by the water flow hit, an impact angle of more than 60° couldn't be tested. Fig. 4 shows the velocity vector of the numerical model inside the feed chamber. The safest inlet angle is not the same for all kinds of set-ups. It may vary according to the design of the chamber and depends on the quality of the membrane. After simulating the flow inside the designed chamber of this study, placing the inlet pipe in various positions and angles, a 60° inlet angle was chosen to be applied. The entry and exit diameters were 15 mm. The membrane properties or the inlet/outlet temperatures were not considered in the simulation as the main focus was to see the fluid flow pattern and observe the washing effect. The fluid flow rate

will influence the velocity profile; therefore, the flow was kept constant at 2 L/min to ensure the pressure inside the chamber did not exceed the membrane liquid entry pressure. The process has been maintained at atmospheric pressure throughout the experiment. The simulation was used to determine the entry angle only; the rest of the work is entirely experimental. Fig. 8 shows the fluid distribution with 60° angled entry to the feed chamber.

4.3. Effect of inlet angle of flow on the production from AGMD system

The earlier flow simulation for modelling the AGMD modules showed the best inlet angle used for the module with maximum safety for the membrane. If the inlet flow hits the membrane directly, especially on the membrane's joints around the chamber wall, the membrane tends to rupture quickly. This limitation restricts any value of the inlet impact angles in the system.

The two surface plots of Fig. 9a and b show the effect of inlet angle when a flat plate has been used. For the discretization of the effect of this one factor only, data was taken on a flat plate first. Later data was also collected with both angled inlet pipe and coolant plate to understand the combined effect and improvement of the whole system. The surface plots show that a maximum of 5.75 kg/m^2·h distillate flux was achieved at 10°C coolant temperature and 70°C feed temperature after using the 60° angled entry, while the straight entry produced 5.01 kg/m^2·h at the same experimental condition. On average, the production rate increased by 10%~17%, implementing the 60° impact angle.

It is also understood from the figures that although the angled entry produced higher distillate flux, the increment rate was not very significant. The reason may be due to the MD process being less sensitive to polarization as it is an evaporative method (no boiling), and there has been constant flow through the chamber. However, the

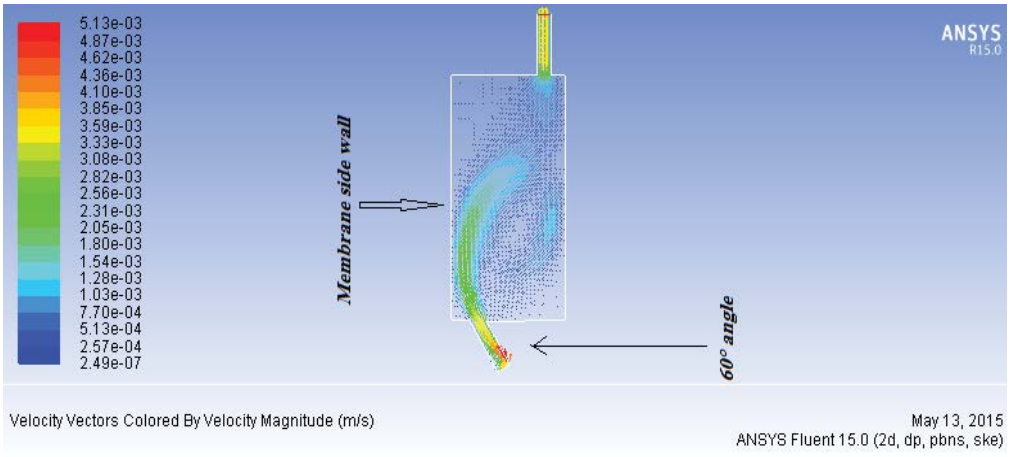

Fig. 8. Flow simulation inside the hot solution chamber to find the impact angle of the inlet pipe.

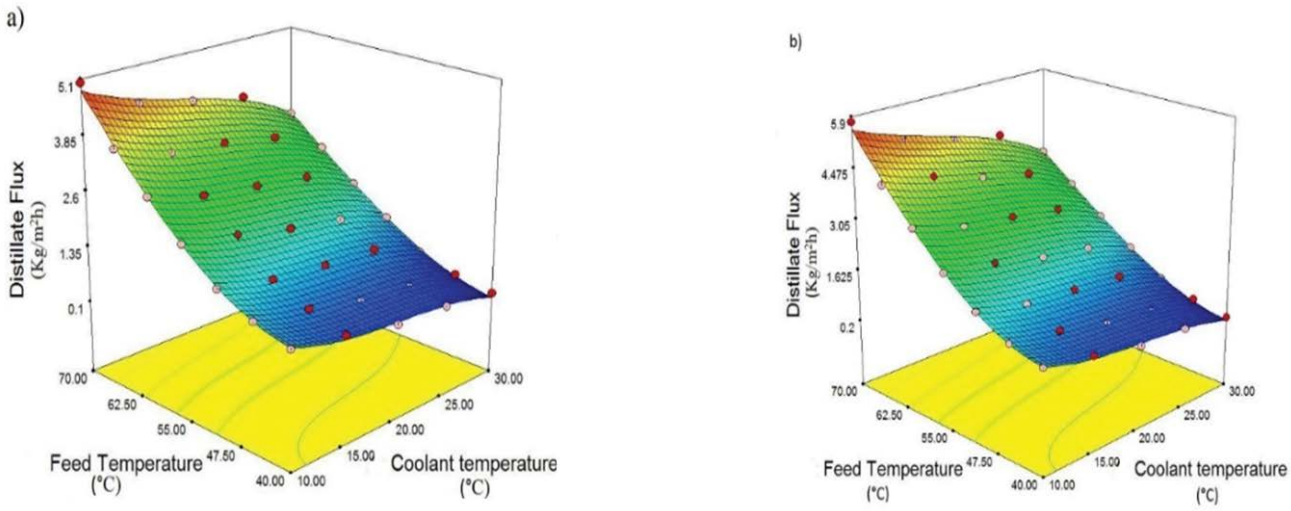

Fig. 9. Surface plot of distillate output for flat coolant plate (a) straight entry inlet flow and (b) 60° angled inlet flow (for flat coolant plate).

improvement of the production rate indicates that the existing polarization was decreased due to the angled entry to the feed chamber. The 'washing effect' near the wall of the membrane doesn't allow the increase of salt concentration around it. So, the concentration polarization decreases consequentially.

4.4. Effect of inlet angle of flow associated with finned coolant plate on the production from AGMD system

As proven from the study, entry angle influences production to a moderate scale and finned coolant plate enhances production significantly; in the next step, the production rate was investigated with a combination of finned coolant plate and inclined feed entry at 60° angle. The distillate production reached up to 8.6 kg/m²·h for the fully modified system, whereas the unmodified system gave a maximum of 5.1 kg/m²·h distillate production for 10°C coolant temperature and 70°C feed side temperature. On average, 68%–78% improvement has been found compared to the normal, unmodified system. The details of production increase for a coolant temperature of 10°C are seen in Table 4. While Fig. 10a and b show the distillate production surface plot and contour plot, respectively, for associating finned coolant plate with inclined feed entry. Therefore, it is summarized from the above study that both coolant plate design and angled entry to the feed chamber will enhance production by different degrees. However, when the angled inlet was combined with the finned coolant plate, the boost in production was significant.

5. Conclusion

The purpose of this study was to experimentally investigate the effect of feed entry angle in an AGMD membrane distillation desalination system. The distillate flux was measured under different operating variables and coolant plate designs. The following statements can be summarized from the study:

- The geometry of the coolant plate has a significant effect on the distillation flux of the AGMD system. The extended active cross-sectional area of the fins provides additional thermal drive to increase the distillate flux. Almost 7.4 kg/m²·h distillate flux has been achieved in the same condition for channelled coolant plate where flat one gives a maximum of 5.1 kg/m²·h at 70°C feed and 10°C coolant temperature. The future scope remains to test the effect of other fin geometries. Especially the circular fins and triangular pin fins can be very effective in minimizing the water droplet entrapment on the top of each fin.
- Tilting the whole module is not a convenient and user-friendly set-up to increase the flux. Providing a large feed entry angle is a perfect solution in this case. The small entry angle has a minor effect on the distillate flux. But it

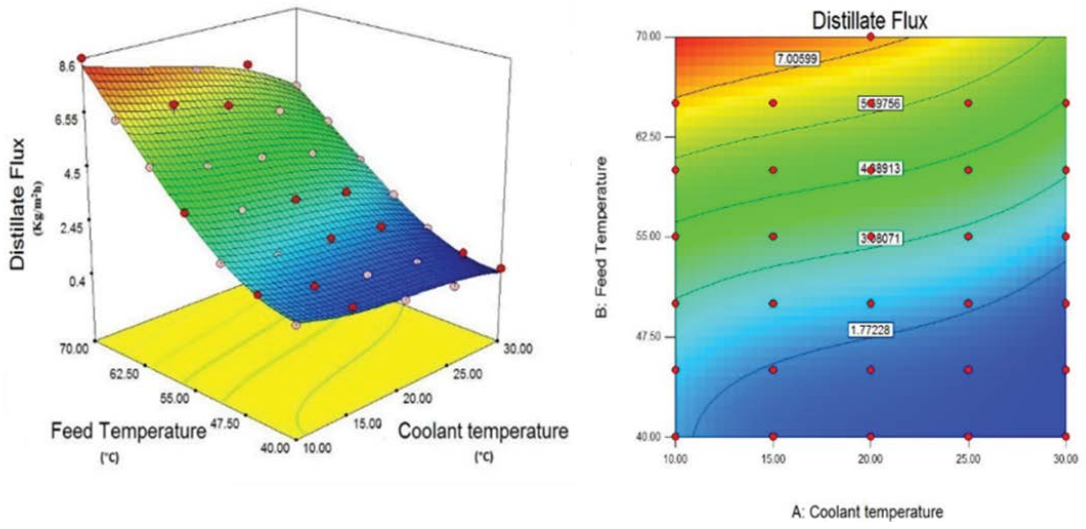

Fig. 10. Distillate flux from the combined finned plate and inclined feed entry (a) surface plot and (b) contour plot.

Table 4
Production for the variable inlet with finned coolant plate for 10 mins (coolant temperature 10°C)

Feed temperature (°C)	40	45	50	55	60	65	70
Distillate collected using straight inlet flow (mL/10 min)	2.3	2.8	3.6	5.0	6.6	8.3	10.9
Distillate collected using 60° angled inlet flow (mL/10 min)	3.9	5.0	6.4	8.9	11.8	14.5	18.6
Performance increase (%)	69.56	78.57	77.78	78.0	78.78	74.7	70.64

becomes quite significant in large angles. Investigations showed that the distillate production increased with a feed entry angle of 60°. The production varies from 10% to 14% in a performance boost, depending upon the feed and coolant temperature. The flow simulation of Fig. 8 shows that the feed solution circulation pattern changes inside the feed chamber when a feed entry angle is provided. At a 60° angle, the feed solution flows more towards the membrane wall and creates a 'washing effect'. So, the salt concentration cannot be increased near the membrane wall. Thus, it decreases concentration polarization.

- With the combined application of 60° angled feed entry and finned coolant plate, an overall 69% to 78% production increase has been achieved for temperatures within the operating range.
- Therefore, the combination of angled entry with a finned coolant plate can enhance the distillate production significantly in an AGMD unit.

Acknowledgments

The authors are grateful to Kulliyyah of Engineering, IIUM, for providing the necessary test facilities. The project was funded by International Islamic University Malaysia's IIUM Endowment fund EDW-B-14-134-1019.

Symbols

A	—	Area, m^2
C	—	Mass concentration, kg/m^3
D	—	Diffusion coefficient, m^2/s
g	—	Gravitational acceleration, m/s^2
h	—	Heat transfer coefficient, $W/(m^2 \cdot K)$
h_f	—	Film height, m
J	—	Flux through membrane, $kg/m^2 \cdot s$
K	—	Thermal conductivity, $W/m \cdot K$
M	—	Molecular weight, kg/mol
$\dot{M}$	—	Mass flow, kg/s
$\hat{m}$	—	Mass flux, kg/s
N	—	Rate of diffusion, mol/s
P	—	Pressure, Pa
Q	—	Heat transfer rate, W
R	—	Universal gas constant, J/k-mol
Ra	—	Rayleigh number
T	—	Temperature, K
V	—	Kinematic viscosity, m^2/s
$\overline{V}$	—	Mean film velocity, m/s
X	—	Thickness of air gap, m
y	—	Year

Greek letters

α	—	Kinematic viscosity, m^2/s
β	—	Thermal expansion coefficient, $W/(m^2 \cdot K)$
δ	—	Condensate film thickness, m
ε	—	Effectiveness
η	—	Efficiency
ρ	—	Density, kg/m^3
Γ	—	Scalar diffusivity, m^2/s

Subscripts

f	—	Film
L	—	Liquid
max	—	Maximum
s	—	Surface
unfin	—	Not finned
v	—	Vapour
w	—	Water

References

[1] M.A. Dawoud, The role of desalination in augmentation of water supply in GCC countries, Desalination, 186 (2005) 187–198.
[2] Quenching Humanity's Freshwater Thirst Creates a Salty Threat – Our World. Available at: https://ourworld.unu.edu/en/quenching-humanitys-freshwater-thirst-creates-a-salty-threat
[3] K.W. Lawson, D.R. Lloyd, Membrane distillation, J. Membr. Sci., 124 (1997) 1–25.
[4] M. Khayet, Membranes and theoretical modeling of membrane distillation: a review, Adv. Colloid Interface Sci., 164 (2011) 56–88.
[5] C.H. Lee, W.H. Hong, Effect of operating variables on the flux and selectivity in sweep gas membrane distillation for dilute aqueous isopropanol, J. Membr. Sci., 188 (2001) 79–86.
[6] A. Alkhudhiri, N. Darwish, N. Hilal, Membrane distillation: a comprehensive review, Desalination, 287 (2012) 2–18.
[7] S.T. Hsu, K.T. Cheng, J.S. Chiou, Seawater desalination by direct contact membrane distillation, Desalination, 143 (2002) 279–287.
[8] M. Khayet, P. Godino, J.I. Mengual, Nature of flow on sweeping gas membrane distillation, J. Membr. Sci., 170 (2000) 243–255.
[9] C.M. Guijt, G.W. Meindersma, T. Reith, A.B. de Haan, Air gap membrane distillation: 2. Model validation and hollow fibre module performance analysis, Sep. Purif. Technol., 43 (2005) 245–255.
[10] M. Khayet Souhaimi, T. Matsuura, Membrane Distillation Principles and Applications, Elsevier, Amsterdam, 2011.
[11] A. Velázquez, J.I. Mengual, Temperature polarization coefficients in membrane distillation, Ind. Eng. Chem. Res., 34 (1995) 585–590.
[12] O.R. Lokare, R.D. Vidic, Impact of operating conditions on measured and predicted concentration polarization in membrane distillation, Environ. Sci. Technol., 53 (2019) 11869–11876.
[13] R.W. Schofield, A.G. Fane, C.J.D. Fell, R. Macoun, Factors affecting flux in membrane distillation, Desalination, 77 (1990) 279–294.
[14] A. Anvari, A. Azimi Yancheshme, K.M. Kekre, A. Ronen, State-of-the-art methods for overcoming temperature polarization in membrane distillation process: a review, J. Membr. Sci., 616 (2020) 118413, doi: 10.1016/j.memsci.2020.118413.
[15] S.M. Alawad, A.E. Khalifa, Performance and energy evaluation of compact multistage air gap membrane distillation system: an experimental investigation, Sep. Purif. Technol., 268 (2021) 118594, doi: 10.1016/j.seppur.2021.118594.
[16] S.M. Alawad, A.E. Khalifa, Development of an efficient compact multistage membrane distillation module for water desalination, Case Stud. Therm. Eng., 25 (2021) 100979, doi: 10.1016/j.csite.2021.100979.
[17] R. Bahar, K.C. Ng, Fresh water production by membrane distillation (MD) using marine engine's waste heat, Sustainable Energy Technol. Assess., 42 (2020) 100860, doi: 10.1016/j.seta.2020.100860.
[18] R. Bahar, M.N.A. Hawlader, T.F. Ariff, Channeled coolant plate: a new method to enhance freshwater production from an air gap membrane distillation (AGMD) desalination unit, Desalination, 359 (2015) 71–81.
[19] A.E. Khalifa, Flux enhanced water gap membrane distillation process-circulation of gap water, Sep. Purif. Technol., 231 (2020) 115938, doi: 10.1016/j.seppur.2019.115938.

[20] D.M. Warsinger, J. Swaminathan, L.L. Morales, J.H. Lienhard V, Comprehensive condensation flow regimes in air gap membrane distillation: visualization and energy efficiency, J. Membr. Sci., 555 (2018) 517–528.
[21] A. Khalifa, D. Lawal, M. Antar, M. Khayet, Experimental and theoretical investigation on water desalination using air gap membrane distillation, Desalination, 376 (2015) 94–108.
[22] D.U. Lawal, A.E. Khalifa, Experimental investigation of an air gap membrane distillation unit with double-sided cooling channel, Desal. Water Treat., 57 (2015) 11066–11080.
[23] D. Lawal, M. Abdul Azeem, A. Khalifa, W. Falath, T. Baroud, M. Antar, Performance improvement of an air gap membrane distillation process with rotating fan, Appl. Therm. Eng., 204 (2022) 117964, doi: 10.1016/j.applthermaleng.2021.117964.
[24] R. Bahar, M.J.P. Bappy, Enhanced production from an air gap membrane distillation desalination system by varying the feed entry angle, IOP Conf. Ser.: Earth Environ. Sci., 945 (2021) 012026.
[25] Effect of Module Inclination Angle on Air Gap Membrane Distillation. Available at: https://dspace.mit.edu/handle/1721.1/100241
[26] H. Kurokawa, O. Kuroda, S. Takahashi, K. Ebara, Vapour permeate characteristics of membrane distillation, Sep. Sci. Technol., 25 (1990) 1349–1359.
[27] J.P. Holman, Heat Transfer, 10th ed., McGraw-Hill, New York, 2010.
[28] A.F. Mills, Basic Heat and Mass Transfer, 2nd ed., Prentice Hall, New Jersey, 1999.
[29] R.K. MacGregor, A.F. Emery, Free convection through vertical plane layers—moderate and high Prandtl number fluids, J. Heat Transfer, 91 (1969) 391–401.
[30] F.P. Incropera, D.P. Dewitt, T.L. Bergman, A.S. Lavine, Introduction to Heat Transfer, 6th ed., John Wiley and Sons Inc., New Jersey, 2011.
[31] A. Fluent, Theory and User's Guide, ANSYS Corporation, Pennsylvania, 2014.
[32] A. Fluent, Theory Guide 14.0, ANSYS Corporation, Pennsylvania, 2011.
[33] M.J. Perves Bappy, R. Bahar, S. Ibrahim, T.F. Ariff, Enhanced freshwater production using finned-plate air gap membrane distillation (AGMD), MATEC Web Conf., 103 (2017) 06014, doi: 10.1051/matecconf/201710306014.
[34] R. Bahar, M.N.A. Hawlader, T.F. Ariff, Channeled coolant plate: a new method to enhance freshwater production from an air gap membrane distillation (AGMD) desalination unit, Desalination, 359 (2015) 71–81.